Measurements of the corneal birefringence with a liquid-crystal imaging polariscope

Juan M. Bueno and Fernando Vargas-Martín

An imaging polariscope has been used to analyze the spatially resolved polarization properties of living human corneas. The apparatus is a modified double-pass setup, incorporating a liquid-crystal modulator in the analyzer pathway. Keeping the incident polarization state fixed (first passage), we recorded a series of three images of the pupil's plane corresponding to independent polarization states of the analyzer unit. Azimuth and retardation at each point of the cornea were calculated from those images. Results show that the magnitude of retardation increases along the radius toward the periphery of the cornea. Left–right eye symmetry in retardation was also found. Maps of azimuth indicate that the direction of the corneal slow axis is nasally downward. © 2002 Optical Society of America

OCIS codes: 120.5410, 170.3880, 330.5370.

1. Introduction

Since the discovery of the corneal birefringence by Brewster,[1] many researchers have used this phenomenon as a tool to investigate the anatomic structure and optical properties of the cornea. Birefringence of the cornea is due to the stroma[2] (composed of layers of collagen fibers, called lamellae), which makes up 90% of the cornea's thickness. The largest contribution to the total ocular retardation has been attributed to the cornea.[3]

Analyzing the change in appearance of the Haidinger brushes when the incoming polarization state was varied, several authors proposed that the eye behaved as a single retardation plate with the slow axis nasally downward.[4–6] Experiments with isolated cat corneas[7] showed that for light incident normally to the corneal surface, the phase retardation is basically zero and increases with the angle of incidence. Bour and Lopes Cardozo[8] psychophysically measured the ocular retardation as a function of the eccentricity of the cornea (in living human eyes), reporting similar results. Taking this fact into account, the cornea was treated as a uniaxial crystal with the optical axis normal to its surface. Using Mueller-matrix ellipsometry, van Blokland and Verhelst[9] measured the corneal birefringence for different positions in the pupil plane of *in vivo* human eyes. They found an approximately fixed retardation at the central area of the pupil plane (larger than zero). At the margins of the pupil (6 mm in diameter) the retardation approached circularly symmetric behavior. They [9] explained the results, assuming that the cornea behaved as a biaxial crystal with its fastest principal axis normal to the corneal surface and its slowest principal axis nasally downward. Pelz and co-workers[10] used the light coming back from the first surface of the lens in order to extract the contribution of the central cornea from the total ocular retardation. Jaronski and Kasprzak found that retardation in human corneas is nearly constant at the center and increases toward the periphery.[11,12] Recent studies have reported that although there is a considerable intraindividual and interindividual variability in corneal parameters (retardation and azimuth),[13,14] the mean corneal polarization axis among normal corneas is nasally downward.

Most of those previous experiments in this area were focused on the central part of the cornea (pupil area). Contributions to the ocular retardation measured across the pupil are mainly due to the cornea and the retina, and it is not easy separate those contributions in the living eye. Despite the usefulness of the Mueller-matrix polarimetry to assess polarization properties of the eye,[10,15–17] polarimetric techniques were not always used.[18–21]

Studies of corneal polarization properties for eccen-

The authors are with the Laboratorio de Óptica, Departament de Física, Universidad de Murcia, Campus de Espinardo, Edificio C, 30071 Murcia, Spain. J. M. Bueno's e-mail address is bueno@um.es.

Received 11 December 2000; revised manuscript received 4 June 2001.

0003-6935/02/010116-09$15.00/0

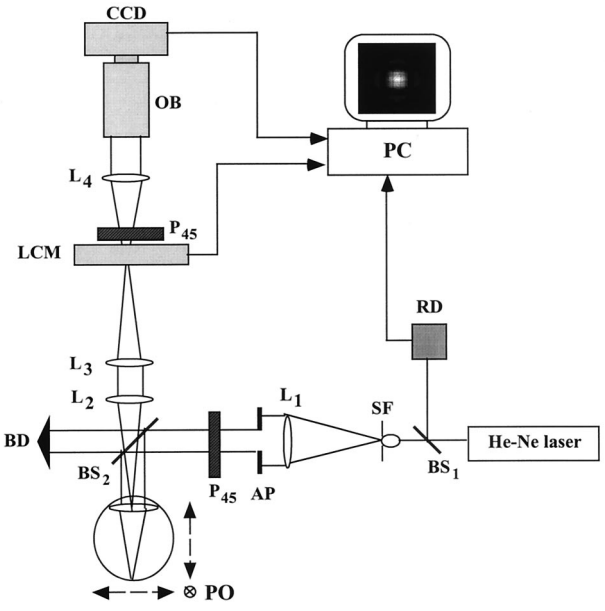

Fig. 1. Schematic diagram of the imaging polariscope. P_{45}, linear polarizers; BS_1 and BS_2, pellicle beam splitters; SF, spatial filter; AP, aperture acting as stop for the first pass; BD, black diffuser; L_1, L_2, L_3, and L_4, achromatic lenses; OB, camera objective; RD, reference detector; PO, micrometric positioner.

tric areas (more than 2.5 mm in radius) have been basically qualitative,[22–25] and quantitative analyses are not numerous.[11,12] In this sense, our aim in this study was to describe more completely the changes in the polarization state of the light double passing the living human cornea and experiencing reflection at the iris. We used a modified double-pass configuration[26] incorporating a liquid-crystal modulator (LCM) in the recording pathway for spatially measuring the parameters of polarization of the cornea (azimuth and retardation).

2. Materials and Methods

A. Experimental Setup

Figure 1 shows a schematic diagram of the experimental apparatus: an imaging polariscope incorporating a LCM (HEX69, Meadowlark Optics) in the exit pathway, adapted to a modified ophthalmoscopic double-pass setup. The eye is illuminated by a 633-nm He–Ne laser beam, filtered and expanded by use of a spatial filter (SF) composed of a microscope objective and a pinhole. Lens L_1 ($f'_1 = 100$ mm) collimates the beam, whose size (12 mm in diameter) is controlled by aperture AP. The beam passes through a linear polarizer (P_{45}) with its transmission axis at 45 deg relative to a horizontal reference and is reflected by a beam splitter (BS_2) before reaching the eye. The fraction of light passing through the pupil's area enters the eye; the rest passes the cornea, experiencing reflection at the iris. In the second passage, lenses L_2 and L_3 ($f'_2 = f'_3 = 500$ mm) conjugate the subject's pupil plane with the plane of a 15-mm-diameter LCM. This LCM and a linear polarizer (parallel to P_{45}) placed behind it act as polarization-state analyzer (PSA). Finally, L_4 ($f'_4 = 600$ mm) and the camera objective make the LCM conjugate with the CCD plane of a slow-scan camera. Reference intensities are recorded by a photodiode (reference detector RD) to correct the mean intensity level in the images, according to fluctuations of the light source. The irradiance on the cornea during exposures was 275 nW/cm^2, several orders of magnitude below the maximum permissible exposure limit.[27] The fast axis of the LCM is vertical, and when driven with appropriate voltages (defined after calibration), three completely independent polarization states are produced.[28] A personal computer controls the voltages applied to the LCM and the CCD camera.

Measurements were carried out in three (well-trained) normal subjects (AB, FV, and PA). The subject's head was stabilized by means of a bite bar mounted on a three-axis micrometric positioner (PO) to align the natural pupil with respect to the incident laser beam.

A series of three images of the pupil's plane (3-s exposure time and 256 × 256 pixels with 14 bits/pixel) were recorded, each corresponding to an independent PSA polarization state. Each pixel of the image corresponds approximately to 0.054 mm in the pupil's plane. Using those images and solving the two mathematical equations presented in Subsection 2.B, we calculated azimuth and retardation at each point of the cornea.

B. Theory: Calculation of α and Δ

In the following, both the theory of the instrument and the method to extract the parameters of polarization of a birefringent sample are explained by use of the Mueller–Stokes formalism. The Mueller matrix of a birefringent sample with retardation Δ and azimuth α (fast axis) is given by[29]:

$$M_\Delta = \begin{bmatrix} 1 & 0 & 0 & 0 \\ 0 & c^2 + s^2 k & sc(1-k) & -sx \\ 0 & sc(1-k) & s^2 + c^2 k & cx \\ 0 & sx & -cx & k \end{bmatrix}, \quad (1)$$

where $c = \cos 2\alpha$, $s = \sin 2\alpha$, $k = \cos \Delta$ and $x = \sin \Delta$.

As a first approximation the global effect due to the living human cornea and the reflection at the iris will be represented by the above matrix. Depolarizing effects due to the nonspecular reflection at the iris are explained in detail in Appendix A.

This Mueller matrix M_Δ^α, transforms the input Stokes vector $\mathbf{S}_{IN}$ with intensity I_p (45-deg linear polarized light) into the output Stokes vector $\mathbf{S}_{OUT}$:

$$\mathbf{S}_{OUT} = \begin{pmatrix} S_0 \\ S_1 \\ S_2 \\ S_3 \end{pmatrix} = I_p \begin{pmatrix} 1 \\ sc(1-k) \\ s^2 + c^2 k \\ -cx \end{pmatrix} = M_\Delta \begin{pmatrix} I_p \\ 0 \\ I_p \\ 0 \end{pmatrix}. \quad (2)$$

If M_{δ}^{90} and M_{p}^{45} are the Mueller matrices for the LCM and the linear polarizer, respectively, the Mueller matrix of the PSA of the exit pathway will be

$$\bar{M}_{\mathrm{PSA}} = M_{p}^{45} M_{\delta}^{90} = \frac{1}{2}\begin{bmatrix} 1 & 0 & \cos\delta & -\sin\delta \\ 0 & 0 & 0 & 0 \\ 1 & 0 & \cos\delta & -\sin\delta \\ 0 & 0 & 0 & 0 \end{bmatrix} \quad (3)$$

where $\delta = \delta_i(V_i)$ is the retardation introduced by the LCM when an external voltage V_i is applied For each δ_i the Stokes vector $\mathbf{S}_{\mathrm{IN}}$ through the entire setup becomes $\mathbf{S}_D^{(i)}$, given by

$$\begin{aligned} \mathbf{S}_D^{(i)} &= \bar{M}_{\mathrm{PSA}}^{(i)} M_{\Delta}^{\alpha} \mathbf{S}_{\mathrm{IN}} \\ &= \frac{1}{2}\begin{pmatrix} S_0 + S_2\cos\delta_i - S_3\sin\delta_i \\ 0 \\ S_0 + S_2\cos\delta_i - S_3\sin\delta_i \\ 0 \end{pmatrix} = \begin{pmatrix} I_F^{(i)} \\ S_1^{D(i)} \\ S_2^{D(i)} \\ S_3^{D(i)} \end{pmatrix}. \end{aligned} \quad (4)$$

The first element of $\mathbf{S}_D^{(i)}$ is the intensity of the image registered by the CCD camera[30] ($I_F^{(i)}$) which depends only on three elements of $\mathbf{S}_{\mathrm{OUT}}$. To obtain those three elements, three independent equations of intensity are required, which is equivalent to using three independent polarization states in the PSA.[28]

Let M_{PSA} be the 3×3 auxiliary matrix with each row being the first row of every $\bar{M}_{\mathrm{PSA}}^{(i)}$ [Eq. (3)] without the null element. This matrix verifies

$$\begin{pmatrix} I_F^{(1)} \\ I_F^{(2)} \\ I_F^{(3)} \end{pmatrix} = \frac{1}{2}\begin{bmatrix} 1 & \cos\delta_1 & -\sin\delta_1 \\ 1 & \cos\delta_2 & -\sin\delta_2 \\ 1 & \cos\delta_3 & -\sin\delta_3 \end{bmatrix}\mathbf{S} = \frac{1}{2} M_{\mathrm{PSA}}\mathbf{S}, \quad (5)$$

where $\mathbf{S} = (S_0, S_2, S_3)^T$ is an auxiliary 3×1 vector (vector $\mathbf{S}_{\mathrm{OUT}}$ without the second element) and δ_i ($i = 1, 2, 3$) are the retardations corresponding to the PSA independent polarization states. A previous calibration of the LCM permits us to calculate those states. A description of this calibration in order to know the relationship between the voltage applied to the LCM and the retardation produced has been described in detail elsewhere.[28,31]

Elements of $\mathbf{S}$ will be obtained by inversion of Eq. (5):

$$\mathbf{S} = \begin{pmatrix} S_0 \\ S_2 \\ S_3 \end{pmatrix} = I_p \begin{pmatrix} 1 \\ s^2 + c^2 k \\ -cx \end{pmatrix} = 2(M_{\mathrm{PSA}})^{-1} \begin{pmatrix} I_F^{(1)} \\ I_F^{(2)} \\ I_F^{(3)} \end{pmatrix}. \quad (6)$$

Normalizing the Stokes parameters of $\mathbf{S}$, operating with the expressions of S_2 and S_3, and using trigonometric relationships, we compute the retardation of the sample under study (Δ) by solving this equation:

$$\bar{A}\cos^2\Delta + \bar{B}\cos\Delta + \bar{C} = 0, \quad (7)$$

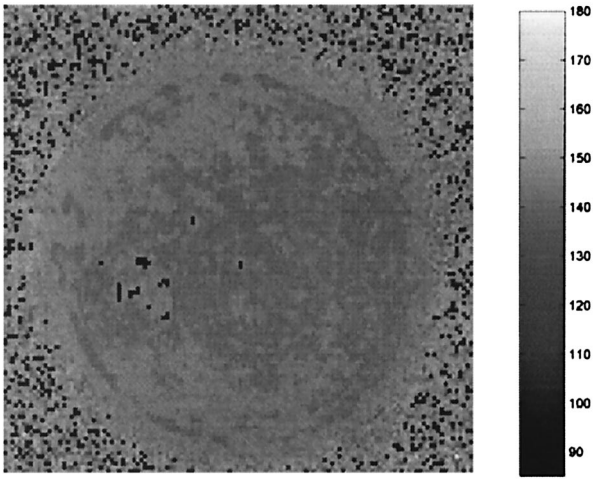

Fig. 2. Distribution of retardation for the test retardation plate in double pass. Image subtends 15 mm. Units are in degrees.

where

$$\begin{aligned} \bar{A} &= S_2 - 1, \\ \bar{B} &= S_3^2, \\ \bar{C} &= -(\bar{A} + \bar{B}). \end{aligned} \quad (8)$$

The nonnull root of Eq. (7) is chosen. Once Δ has been calculated, the azimuth of the fast axis of the sample under study (α) will be obtained as

$$\alpha = \frac{1}{2}\, a\, \cos\left(-\frac{S_3}{\sin\Delta}\right). \quad (9)$$

3. Results

A. Calibrations

First, the complete setup was calibrated to verify the performance of the experimental system. With Eq. (6), the 3×1 vector $\mathbf{S}$ obtained when a 45-deg linear polarized light entered the PSA was $(S_0 = 1, S_2 = 0.98, S_3 = -0.01)^T$ [vector $(1, 1, 0)^T$ was expected].

The experimental apparatus was used to calculate both the spatially resolved azimuth and retardation of a commercially available quarter-wave plate (for 543 nm, expected retardation 154 deg) in double pass. For this operation the retardation plate and a mirror were placed in the place of the eye. Three images (0.5-s exposure) each corresponding to an independent retardation of the LCM were recorded. The parameters were calculated at each pixel in the image with Eqs. (6)–(9). Figure 2 shows the map for the retardation (mean 156.3 deg, standard deviation ± 2.9). In Fig. 3 spatially resolved azimuths (fast axes) for two different orientations of the plate are also presented. Systematic errors (estimated at 1–3%) obtained with these calibrations are similar to those previously presented in the literature.[10,16,17,28,32–37]

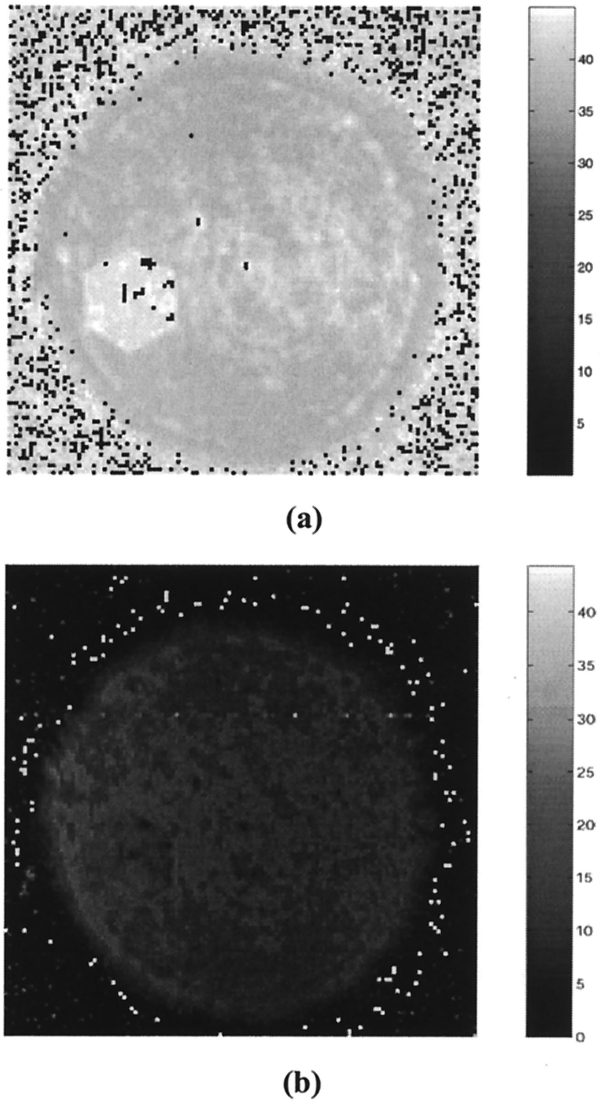

Fig. 3. Spatially resolved azimuth (deg) for two different orientations of the fast axis of the retarder used for calibration: (a) 40 and (b) 0 deg. Averages: (a) 38.1 ± 2.0 deg (b) 2.4 ± 1.2 deg.

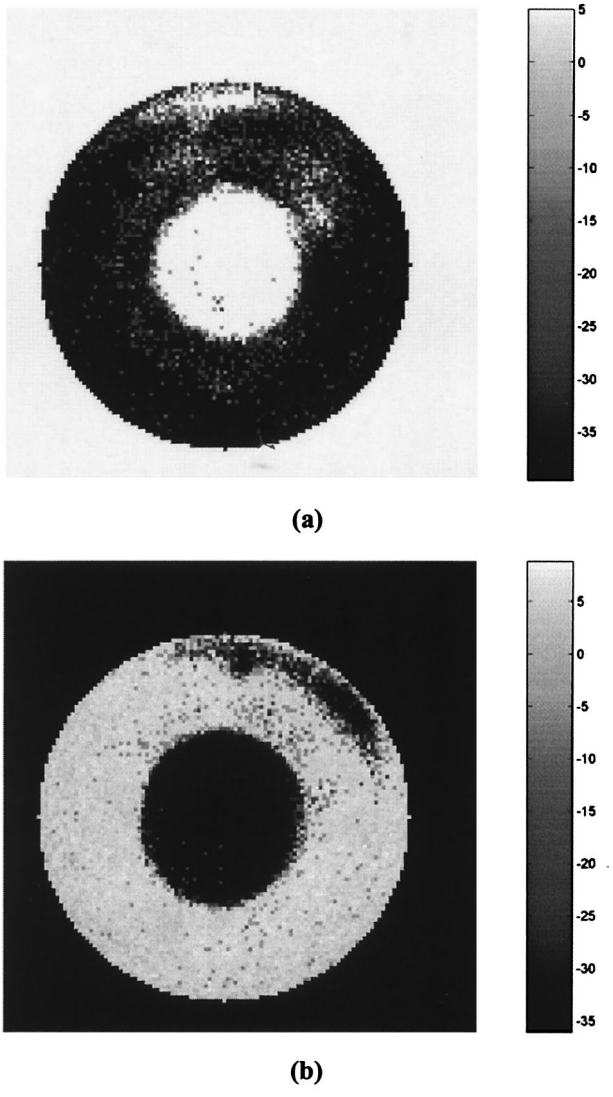

Fig. 4. Orientation of the slow axis (in degrees) for the two eyes of subject PA: (a) right eye, (b) left eye. Zero is horizontal, and the angle increases counterclockwise when looking into the eye. Each image has a full size of 13.8 mm.

B. Polarization Parameters for Living Human Corneas

A series of three images of the pupil plane corresponding to the three independent PSA polarization states were recorded for each subject. With each series and again with the set of Eqs. (6)–(9), retardation and azimuth at each pixel were calculated. These parameters correspond to the magnitude of the retardation introduced by the cornea at each imaged point and the azimuth of the eigenvector associated with its birefringent structure. Only light coming back from the iris has been taken into account (neither points inside the area of the pupil nor points of the sclera). Figure 4 presents the spatially resolved azimuth (slow axis) for the two eyes of subject PA. This figure shows that the direction of the corneal slow axis is nasally downward. The parameter is almost uniform across the image. Circular areas in the middle of the images correspond to the pupil and have not been analyzed. To check the possible symmetry between both eyes, values of azimuth along two different meridians of the image for two subjects have been plotted in Fig. 5.

The distribution of retardation introduced at each point by the cornea (double passage) is presented in Fig. 6 for one of the subjects. For a better discrimination, retardations along two meridians of the image (horizontal and vertical) are displayed in Fig. 7. Results for ±45-deg meridians (not shown in the figure) were similar. This parameter reflects the fluctuations of corneal thickness and local disturbances in corneal structure. This retardation associated with corneal birefringence presents an approximately symmetric behavior around the center of the pupil and increases toward the periphery. The radial averaged corneal retardation profile for FV is shown in Fig. 8. To obtain this one-dimensional

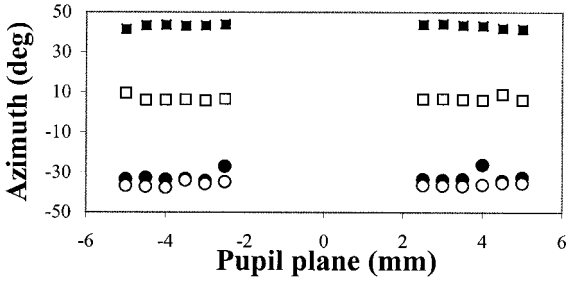

Fig. 5. Values of azimuth along a horizontal meridian for two different subjects: AB, filled symbols; PA, open symbols; squares, left eye; circles, right eyes. Negative distances indicate temporal and nasal sides for right and left eyes, respectively.

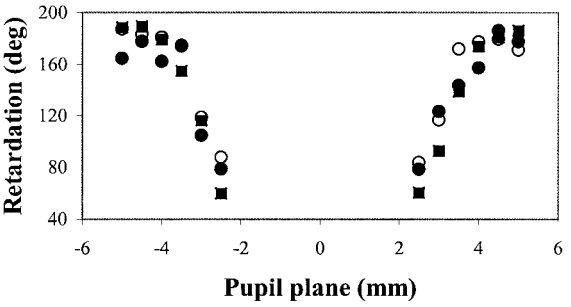

Fig. 7. Corneal retardation along two meridians of the image for subject PA (filled circles, vertical; open circles, horizontal) and one meridian for AB (squares, horizontal). Data correspond to right eyes. Negative distances represent temporal side.

plot, values for a fixed radial distance to the center of the image were integrated and then averaged in all directions.

The comparison between the retardation associated with both left and right eyes for one of the subjects is presented in Fig. 9. This plot shows the left–right symmetry in retardation for both eyes in the same subject.

4. Discussion and Conclusions

An imaging polariscope incorporating a LCM in the analyzer pathway has been developed to measure polarization parameters of *in vivo* human corneas. Parameters are computed by solution of two mathematical equations. In general, this setup can also be used for the analysis of any nondichroic linear retarder such as some crystals (i.e., quartz) or form birefringent samples (i.e., some physiological liquids or tissues). LCMs have been previously used in many applications.[37–44] Moreover, these devices have recently been applied to measure polarization properties of the human eye.[16,17,45,46]

The light double passing the eye changes its polarization state. Those changes are mainly due to the linear birefringence of the cornea[3,19] and can be represented by a rotation on the Poincaré sphere[29] around the eigenvector of the equivalent retarder. If only the light reflected at the iris is registered, effects of the light going through the ocular media and experiencing reflection in the retina are avoided, and the influence of the cornea itself on the modification of the polarization state can be studied. The effects of depolarization due to the reflection at the iris are shown in Appendix A.

Maps of corneal azimuth in Fig. 4 are quite uniform. The orientation of the eigenvector is along the upper-temporal to lower-nasal direction. These results agree with those previously obtained[4,5,10] that proposed a slow axis with an inclination with the horizontal ranging from 0 to 40 deg. Although Greenfield and co-workers reported a bigger range for the central corneal axis orientation of 118 eyes in 63 subjects, the mean corneal polarization slow axis was also along the same direction.[13] For the subjects used in this study the orientation of the slow axis ranged from 5 to 45 deg (positive or negative depending on the eye). In addition, Fig. 5 shows a lack of symmetry between both eyes in the orientation of the corneal slow axis. Van Blokland and Verhelst[9] found an orientation similar only at the central cornea. They also proposed a nonsignificant left–right symmetry and substantial interindividual differences. This slow axis orientation contrasts with the radial distribution previously reported.[8,47] A recent

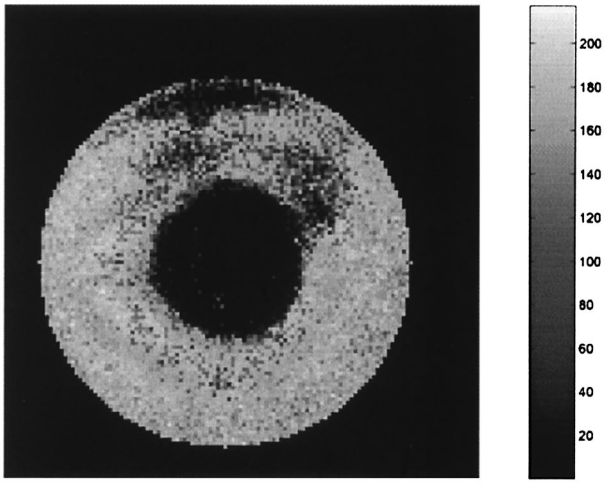

Fig. 6. Spatially resolved retardation for the cornea of subject PA. Units are in degrees.

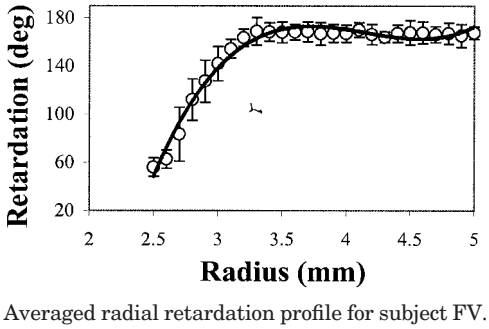

Fig. 8. Averaged radial retardation profile for subject FV. Error bars represent the standard deviation. Black curve represents the corresponding third polynomial fitting.

study for *in vitro* corneas also presented some uniformity for the distribution of azimuth.[48]

The corneal stroma is composed of ~100 layers of parallel fibers (lamellae).[19] Stanworth and Naylor first proposed an approximately random lamellar arrangement,[7,47] which was interpreted as an absence of a preferential direction in the cornea. In contrast, other *in vivo* and *in vitro* experiments proposed a preferential orientation of the lamellae.[24,49–52] Maurice[2] noted that many species exhibit behavior typical of a biaxial crystal, which suggested that lamellae are not completely oriented at random but tend to lie in one direction. The biaxility proposed in Ref. 9 was attributed to a preferred lamellar direction that is, in general, nasally downward. Theoretical simulations by Donohue and colleagues confirmed that the lamellae orientations are not entirely random, but rather a significant fraction are oriented in a fixed, preferred direction.[53] Their mathematical model is applicable to any location of the corneal surface. Our results agree with the existence of that preferential orientation.

Figures 6–8 display the behavior of the corneal retardation between 2.5 and 5 mm in radius. Although the magnitude of retardation depends on the subjects, it increases from the center to the periphery. A minimum (nonnull) is observable at the edge of the pupil. In addition, the retardation along the radius follows a cubic polynomial curve ($R = 0.98, 0.98, 0.97$ and $p < 0.0001$ for AB, FV, and PA, respectively).

Some authors modeled the effect of the ocular media as a fixed retardation plate,[4–6] measuring retardations between 30 and 90 deg. Other researchers reported that the amount of retardation increased from zero in the center of the pupil to approximately 50–100 deg at the margins,[8,47] although a larger increase in retardation for the diagonal meridians than for the horizontal and vertical meridians was found. Posterior experiments[9] showed that the corneal retardation was different from zero and approximately constant at the central area of the pupil plane (55 deg on average). The retardation was also reported to increase in the superior and inferior directions (for some subjects at approximately 175–200 deg at the edges of a 6-mm pupil) and to decrease toward the nasal and temporal parts of the pupil. Measurements for *in vitro* corneas showed an increase in retardation toward the periphery.[7,11,48,49]

The model reported by van Blokland and Verhelst[9] deserves special attention. In that study the corneal axis was oriented downward nasally at the central area but tended toward a tangential orientation at the margins of the pupil. The central cornea showed a fixed retardation, but the parameter decreased in the temporal and nasal direction, and it increased when going toward the superior and inferior parts of the pupil (saddlebacklike distribution). There are also two points of zero retardation located diametrically across the pupil. In view of this, authors proposed that the cornea behaved as a biaxial crystal. The proposed model tried to solve the two conflicting models to describe the ocular retardation (see Ref. 9 for more details). The model of van Blokland and Verhelst[9] seemed to match fairly well their own data but not all the previous corneal studies. In particular, those results were different from those presented by Bour and Lopes Cardozo[8] some years before. The latter measured the ocular retardation for the same area of the pupil and found an increase in retardation toward the periphery for different meridians. In addition, they found neither points of zero retardation nor a decrease in temporal and nasal sides. Posterior experiments have also proposed a symmetric increase in retardation toward the limbus.[11,48] Recent results have reported central corneal retardations ranging from 0 to 190 nm depending on the subject,[14] which shows the large variability among subjects. In their study van Blokland and Verhelst stated that retardations at the edges of the pupil show no transience with the retardation obtained from polarization patterns of the iris recorded with circular light.[9] That fact is also present in our case: We measured the ocular retardation at the central cornea for two pupil sizes[17] in the right eye of subject PA, obtaining values of 64.5 and 86.8 deg for 2 and 5 mm, respectively.

Reasons for differences between the results with the biaxial model and the present ones are not completely clear, and, at this point, we cannot make a direct comparison. In the following we discuss a set of experimental issues that could have influenced the calculation of the corneal parameters in that previous study.

At the pupil plane a spatial variation of the degree of polarization associated with the two components on the light reflected back from the retina has been reported.[46,54,55] The maximum for that parameter is located close to the peak of the guided component, and it does not always correspond to the center of the pupil. Authors van Blokland and van Norren[54] measured a decrease of only 10% in a 6-mm pupil; however, other authors have found a much larger reduction for both medium[55] and long wavelengths.[46] If a decrease in the degree of polarization is associated with an increase in the error in the determination of the retardation and the azimuth,[9] and for eccentric areas of the pupil, the parameter value is lower than that reported in Ref. 54; this could have had a large influence on the results (retardation and azimuth).

The biaxial model is closely related to the presence of an elliptical retarder at the peripheral cornea; however, spatially resolved polarimetry of the cornea has shown linear birefringence.[48] Other experimenters have also reported that the ocular birefringence assessed with different light-beam diameters is also linear.[17] Additionally, even though the model agrees with the distribution of retardation, it fails to explain the presence of elliptical birefringence.

It is thought that the influence of the lenticular retardation is much smaller than that corresponding to the cornea. *In vitro* analyses[56] have shown a retardation of 8 deg (on average) for a single pass and a pattern for the azimuth that depends on both the

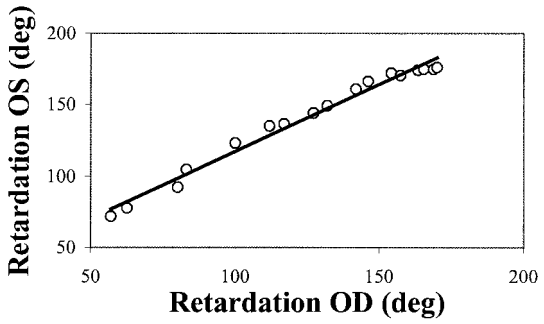

Fig. 9. Right (OD) versus left eye (OS) retardation for subject FV. Solid line represents the linear fit to the data.

area of the lens and the specimen. This implies that the light passing through different parts of the lens will have a different influence on the total ocular retardation, depending on the relative orientation of the lenticular and corneal axes. This issue is probably less important than the previous ones, but it might explain the shift in the origin of the saddleback function of Ref. 9, where the model also fails.

There is a direct relationship between the retardation associated with a birefringent structure and its thickness.[57] The increase in corneal thickness along the radius is not as large as the increase in retardation.[58] This could indicate that variations in retardation are due not only to an increment in corneal thickness but also to changes in the corneal birefringence with the eccentricity,[9,49] although corneal curvature could also be a reason for an increase in the observed retardation.[49]

When left–right symmetry is taken into account (Fig. 9), the retardation has a common behavior ($R = 0.99$, $p < 0.0001$, $\alpha = 0.97$). Symmetry in retardation is more significant than in azimuth. This confirms previous experiments for the pupil's area,[9] although an extension to large eccentricities is given here.

In general, spatial distributions allow for a more complete description of spatial changes in the polarization state of the light passing through the cornea. Investigation of the corneal birefringence could be useful in medical diagnosis of corneal pathologies (i.e., keratoconus) and have some potential applications in refractive surgery procedures and corneal transplantation. This analysis would also permit an examination of the corneal structure and lamellar arrangement as well as the study of the phenomena of stress-induced birefringence.[59]

To summarize, retardation and azimuth of *in vivo* corneas have been calculated by use of a liquid-crystal imaging polariscope. Results show that the slow axis of the corneal birefringent structure is in general nasally downward, although interindividual differences occur. This could be associated with a preferential orientation in the lamellar distribution. The magnitude of retardation increases from the center of the cornea toward the limbus, indicating an increase in both corneal thickness and birefringence. The applications of this kind of experimental system to a clinical environment might be oriented to test both corneal pathologies and structural changes following surgery.

Appendix A

In this study we have assumed the validity of Eq. (1) for describing the polarization properties of the *in vivo* human cornea. That equation describes the effect of the cornea and the reflection in the iris as a purely linear birefringent material. Spatial corneal birefringence was recently reported to be linear.[48] However, the iris does not behave as a specular reflector, which implies the existence of depolarizing effects probably associated with scattering and diffusion. In the following we present the expressions required for extracting the parameters of polarization when effects of depolarization are included. We also show how this issue affects the present results.

The depolarizing effects of the iris are incorporated by addition of the contribution of the Mueller matrix for a depolarizer[60] (M_g). Taking into account the decomposition theorem reported by Lu and Chipman,[61] the Mueller matrix corresponding to the system iris + cornea will be result of the product $M_g M_\Delta^\alpha$. Then the corresponding Stokes vector emerging from the cornea $\mathbf{S}_{\mathrm{OUT}}^{(g)}$ will be

$$\mathbf{S}_{\mathrm{OUT}}^{(g)} = \begin{pmatrix} S_0^{(g)} \\ S_1^{(g)} \\ S_2^{(g)} \\ S_3^{(g)} \end{pmatrix} = I_p \begin{pmatrix} 1 \\ gsc(1-k) \\ g(s^2 + c^2 k) \\ -gcx \end{pmatrix} = M_g M_\Delta^\alpha \begin{pmatrix} I_p \\ 0 \\ I_p \\ 0 \end{pmatrix}, \quad \text{(A1)}$$

where g is the degree of polarization of the light beam.

Operating as we did in Subsection 2.B, the corneal retardation (Δ) can be calculated by means of an equation similar to Eq. (7):

$$\bar{A}_g \cos^2 \Delta + \bar{B}_g \cos \Delta + \bar{C}_g = 0, \quad \text{(A2)}$$

where now

$$\begin{aligned} \bar{A}_g &= gS_2 - g^2, \\ \bar{B}_g &= S_3^2, \\ \bar{C}_g &= -(\bar{A}_g + \bar{B}_g). \end{aligned} \quad \text{(A3)}$$

The azimuth (α) can be obtained as

$$\alpha = \frac{1}{2}\,\alpha\,\cos\left[-\frac{S_3}{g(\sin\Delta)}\right]. \quad \text{(A4)}$$

For the calculation of the degree of polarization of a light beam (g in this case), the whole Stokes vector is required.[60] Since a LCM provides only three independent polarization states,[28] we will never be able to calculate the four elements of the Stokes vector.

In particular, studies about the effect of depolarization of the human iris have not been reported to our knowledge. Cope and colleagues claimed only (after a qualitative analysis) that the iris does not completely depolarize the light.[24] Thus no quanti-

Table 1. Errors Introduced in the Calculation of Corneal Parameters when Depolarizing Properties of the Iris Are Not Taken into Account[a]

Degree of Polarization	Corneal Thickness Increment (μm)	Corneal Polarization Axis Increment (deg)
0.9	2.5 ± 1.8	3.5 ± 3.8
0.8	4.8 ± 3.4	6.9 ± 4.7
0.7	6.9 ± 5.5	8.9 ± 6.0
0.6	8.9 ± 7.6	10.8 ± 4.4
0.5	10.8 ± 9.7	12.5 ± 3.5

[a]Increment means the difference (absolute value) between calculated [with Eqs. (7)–(9)] and expected values [with Eqs. (A2)–(A4)].

tative references on that issue can be taken into account. When we look at the cornea (iris) between both parallel and crossed linear polarizers, its appearance is different. If the emergent light is almost depolarized, the intensity registered during rotation of the analyzer would be almost constant; however, that does not happen: Changes in intensity patterns are clearly seen, and the corneal cross appears only when the transmission axes of polarizers are 90 deg apart.

In the following we check the effect of those depolarizing effects in the results that we have obtained in this paper. For that purpose we modeled the cornea as a birefringent plate with retardation ranging from 40 to 90 deg (simple pass) and azimuth between ±10 and ±55 deg.[19] The iris was modeled as a depolarizer with degree of polarization ranging from 0.9 to 0.5 (increments of 0.1). Stokes vectors corresponding to the different combinations cornea + iris were computed, and the corneal parameters were extracted with Eqs. (7)–(9). Those parameters were compared with the ideal retardations and azimuths obtained with Eqs. (A2)–(A4).

Table 1 shows the averaged results for each degree of polarization. In general, errors (differences between calculated and expected values) in the calculation of both parameters increase with depolarization. Increments (absolute value) in the azimuthal angle as a function of the degree of polarization of the iris are expressed in degrees. With data of birefringence from the bibliography,[19] results for the retardation have been converted to corneal thickness for better understand the phenomenon.

Averaged corneal thickness have been reported to increase gradually for 501 μm at the center to 726 μm at 5 mm of radial eccentricity.[62] This means that even in our worst case (depolarization of 0.5 and central cornea, where we do not even have data) the fact of not taking into account the depolarization effect of the iris would represent an error of 4% in the computed corneal thickness. For an eccentricity of 2.5 mm the error would reduce to 3.5%. As a first approximation this indicates that the method described here might be useful for the assessment of corneal parameters mainly oriented toward clinical applications.

This research was partially supported by Dirección General de Enseñanza Superior (Spain) grant PB97–1056 to P. Artal. Experimental measurements reported in this paper were performed at the University of Murcia (Spain). The imaging analysis and the writing of the manuscript were carried out at the School of Optometry (University of Waterloo, Ontario, Canada) and the Schepens Eye Research Institute (Boston, Mass.) while the authors were supported by postdoctoral fellowships. The authors gratefully acknowledge P. Artal for helpful suggestions on the first steps of the experiment and for providing the LCM and the rest of technical and optical elements used for building the experimental setup used in this study.

References

1. D. Brewster, "Experiments on the de-polarization of light as exhibited by various mineral, animal and vegetable bodies with a reference of the phenomena to the general principles of polarization," Philos. Trans. R. Soc. London **1,** 21–53 (1815).
2. D. M. Maurice, "The cornea and sclera," in *The Eye*, H. Davson, ed. (Academic, Orlando, Fla., 1984), pp. 1–158.
3. G. J. van Blokland, "The optics of the human eye studied with respect to polarized light," Ph.D. dissertation (University of Utrecht, Utrecht, The Netherlands, 1986).
4. G. Boehm, "Ueber maculare (Haidingersche) Polarisations buschel und ueber einen polarisationoptischen Fehler des Auges," Acta Ophthalmol. **18,** 109–169 (1940).
5. H. L. de Vries, A. Spoor, and R. Jielof, "Properties of the eye with respect to polarized light," Physica **19,** 419–432 (1953).
6. E. J. Naylor and A. Stanworth, "Retinal pigment and the Haidinger effect," J. Physiol. **124,** 543–552 (1954).
7. A. Stanworth and E. J. Naylor, "The polarization optics of the isolated cornea," Br. J. Ophthal. **34,** 201–211 (1950).
8. L. J. Bour and N. J. Lopes Cardozo, "On the birefringence of the living human eye," Vision Res. **21,** 1413–1421 (1981).
9. G. J. van Blokland and S. C. Verhelst, "Corneal polarization in the living human eye explained with a biaxial model," J. Opt. Soc. Am. A **4,** 82–90 (1987).
10. B. Pelz, C. Weschenmoser, S. Goelz, J. P. Fischer, R. O. W. Burk, and J. F. Bille, "*In vivo* measurement of the retinal birefringence with regard on corneal effects using an electro-optical ellipsometer," in *Lasers in Ophthalmology IV*, R. Birngruber, A. F. Fercher, and P. Sourdille, eds., Proc. SPIE **2930,** 92–101 (1996).
11. J. W. Jaronski, H. T. Kasprzak, D. Haszcz, and J. Zagorski, "Investigation of the corneal structure by use of phase stepping imaging polarimetry," in *Proceedings of the European Optical Society Topical Meeting in Physiological Optics* (European Optical Society, Wroclaw, Poland, 1999), pp. 21–22.
12. J. W. Jaronski and H. T. Kasprzak, "Generalized algorithm for photoelastic measurements based on phase-stepping imaging polarimetry," Appl. Opt. **38,** 7018–7025 (1999).
13. D. S. Greenfield, R. W. Knighton, and X.-R. Huang, "Effect of corneal polarization axis on assessment of retinal nerve fiber layer thickness by scanning laser polarimetry," Am. J. Ophthalmol. **129,** 715–722 (2000).
14. R. W. Knighton, X.-R. Huang, and D. S. Greenfield, "Linear birefringence measured in the central corneas of a normal population," Invest. Ophthalmol. Visual Sci. (Suppl.) **42,** S131 (2001).
15. G. J. van Blokland, "Ellipsometry of the human retina *in vivo*: preservation of polarization," J. Opt. Soc. Am. A **2,** 72–75 (1985).

16. J. M. Bueno and P. Artal, "Double-pass imaging polarimetry in the human eye," Opt. Lett. **24,** 64–66 (1999).
17. J. M. Bueno, "Measurement of parameters of polarization in the living human eye using imaging polarimetry," Vision Res. **40,** 3791–3799 (2000).
18. F. A. Bettelheim and K. Mahadeva, "An interpretation of small-angle light-scattering patterns of human cornea," Invest. Ophthalmol. Visual Sci. **16,** 233–236 (1977).
19. L. J. Bour, "Polarized light and the eye," in *Vision Optics and Instrumentation*, W. N. Charman, ed. (CRC Press, Boston, Mass., 1991), Vol. 1, Chap. 13.
20. R. L. McCally, W. J. Green, W. A. Chistens-Barry, D. J. Donohue, and R. A. Farrell, "Birefringence properties of human and rabbit cornea: polarization rotation component," Invest. Ophthalmol. Visual Sci. (Suppl.) **37,** S1007 (1996).
21. R. A. Farrell and R. L. McCally, "Corneal lamelar birefringence—effects of fibril anisotropic permittivity on retardation," Invest. Ophthalmol. Visual Sci. (Suppl.) **38,** S505 (1997).
22. D. G. Cogan, "Some ocular phenomena produced with polarized light," Arch. Ophthalmol. (Chicago) **25,** 391–400 (1941).
23. G. W. Nyquist, "Stress-induced birefringence of the cornea," Am. J. Ophthalmol. **65,** 398–404 (1968).
24. W. T. Cope, M. L. Wolbarsht, and B. S. Yamanashi, "The corneal polarization cross," J. Opt. Soc. Am. **68,** 1139–1141. (1978).
25. Y. Ichihashi, M. H. Khin, K. Ishikawa, and T. Hatada, "Birefringence effect of the *in vivo* cornea," Opt. Eng. **34,** 693–699 (1995).
26. J. Santamaría, P. Artal, and J. Bescós, "Determination of the point-spread function of human eyes using a hybrid optical-digital method," J. Opt. Soc. Am. A **4,** 1109–1114 (1987).
27. American National Standard for the Safe Use of Lasers ANSI Z136.1. (Laser Institute of America, Orlando, Fla., 1993).
28. J. M. Bueno, "Polarimetry using liquid-crystal variable retarders: theory and calibration," J. Opt. A **2,** 216–222 (2000).
29. D. S. Kliger, J. W. Lewis, and C. E. Randall, "*Polarized Light in Optics and Spectroscopy* (Academic, San Diego, Calif., 1990).
30. W. A. Shurcliff, "*Polarized Light: Production and Use* (Harvard University, Cambridge, Mass., 1962).
31. F. Vargas-Martín, "Óptica adaptativa en oftalmoscopia: corrección de las aberraciones del ojo mediante un modulador espacial de cristal líquido," Tesis Doctoral (Universidad de Murcia, Murcia, Spain, 1999).
32. R. C. Thompson, J. R. Bottinger, and E. S. Fry, "Measurement of polarized light interactions via the Mueller matrix," Appl. Opt. **19,** 1323–1332 (1980).
33. E. Bernabeu and J. J. Gil, "An experimental device for the dynamic determination of Mueller matrices," J. Opt. (Paris) **16,** 139–141 (1985).
34. D. H. Goldstein and R. A. Chipman, "Error analysis of a Mueller matrix polarimeter," J. Opt. Soc. Am. A **7,** 693–700 (1990).
35. T. Fendrich, "Fourierellipsometrie," Diplomarbeit (Universität Heidelberg, Heidelberg, Germany, 1991).
36. F. Delplancke, "Automated high-speed Mueller matrix scatterometer," Appl. Opt. **36,** 5388–5395 (1997).
37. C. Wu and S. Wu, "Liquid-crystal-based switchable polarizers for sensor protection," Appl. Opt. **34,** 7221–7227 (1995).
38. C. Ye, "Construction of an optical rotator using quarter-wave plates and an optical retarder," Opt. Eng. **34,** 3031–3035 (1995).
39. S. Krishnan and P. C. Nordine, "Fast ellipsometry and Mueller matrix ellipsometry using the division-of-amplitude photopolarimeter," in *International Symposium on Polarization Analysis and Applications to Device Technology*, T. Yoshizawa and H. Yokota, eds., Proc. SPIE **2873,** 152–156 (1996).
40. J. Liu and R. M. A. Azzam, "Polarization properties of corner-cube retroreflectors: theory and experiment," Appl. Opt. **36,** 1553–1559 (1997).
41. C. Ye and E. Keränen, "Nonmechanical rotation of a linear polarizer preceding a photodetector," J. Opt. Soc. Am. A **14,** 682–685 (1997).
42. G. D. Love, "Wave-front correction and production of Zernike modes with a liquid-crystal spatial light modulator," Appl. Opt. **36,** 1517–1524 (1997).
43. F. Vargas-Martín, P. Prieto, and P. Artal, "Correction of the aberrations in the human eye with a liquid-crystal spatial light modulator: limits to performance," J. Opt. Soc. Am. A **15,** 2552–2562 (1998).
44. Z. Zhuang, S.-W. Suh, and J. S. Patel, "Polarization controller using nematic liquid crystals," Opt. Lett. **24,** 694–696 (1999).
45. J. M. Bueno and P. Artal, "Polarization and retinal image quality estimates in the human eye," J. Opt. Soc. Am. A **18,** 489–496 (2001).
46. J. M. Bueno, "Depolarization effects in the human eye," Vision Res. **41,** 2687–2696 (2001).
47. A. Stanworth and E. J. Naylor, "Polarized light studies of the cornea," J. Exp. Biol. **30,** 160–169 (1953).
48. J. M. Bueno and J. W. Jaronski, "Spatially resolved polarization properties for *in vitro* corneas," Ophthal. Physiol. Opt. **21,** 384–392 (2001).
49. D. Kaplan and F. A. Bettelheim, "On the birefringence of bovine cornea," Exp. Eye Res. **13,** 219–226 (1972).
50. D. Post and J. E. Gurland, "Birefringence of the cat cornea," Exp. Eye Res. **5,** 286–295 (1966).
51. C. C. D. Shute, "Haidinger's brushes and predominant orientation of collagen in corneal stroma" Nature (London) **250,** 163–164 (1974).
52. R. L. McCally and R. A. Farrell, "Structural implications of the small-angle light scattering from the cornea," Exp. Eye Res. **34,** 99–113 (1982).
53. D. J. Donohue, B. J. Stoyanov, R. L. McCally, and R. A. Farrell, "Numerical modeling of the cornea's lamellar structure and birefringence properties," J. Opt. Soc. Am. A **12,** 1425–1438 (1995).
54. G. J. van Blokland and D. van Norren, "Intensity and polarization of light scattered at small angles from the human fovea," Vision Res. **26,** 485–494 (1986).
55. S. A. Burns, S. Wu, S. F. C. Delori, and A. E. Elsner, "Direct measurement of human-cone-photoreceptor alignment," J. Opt. Soc. Am. A **12,** 2329–2338 (1995).
56. J. M. Bueno and M. C. W. Campbell, "Polarization properties for in vitro human lenses," Invest. Ophthalmol. Visual Sci. (Suppl.) **42,** S161 (2001).
57. M. Born and E. Wolf, "*Principles of Optics* (Pergamon Press, New York, 6th ed., 1980).
58. D. Fonn, J. H. Wang, and T. L. Simpson, "Topographical thickness of the epithelium and the total cornea in living human eyes using optical coherence tomography," Invest. Ophthalmol. Vis. Sci. (Suppl.) **41,** S675 (2000).
59. S. J. Haake and E. A. Patterson, "Photoelastic anaalysis of frozen stressed specimens using spectral contents analysis," Exp. Mech. **32,** 266–272 (1992).
60. R. A. Chipman, "Polarimetry," in *Handbook of Optics*, 2nd ed., M. Bass, ed. (McGraw-Hill, New York, 1995), Vol. 2, Chap. 22.
61. S. Lu and R. A. Chipman, "Interpretation of Mueller matrices based on polar decomposition," J. Opt. Soc. Am. A **13,** 1106–1113 (1996).
62. J. H. Wang, "Corneal and epithelial thickness changes associated with contact lens wear and eye closure comparing optical coherence tomography and optical pachometry," M.S. thesis (University of Waterloo, Waterloo, Ontario, 2000).